J Mater Sci (2009) 44:4959–4968
DOI 10.1007/s10853-009-3758-3

Water-based sol–gel nanocrystalline barium titanate: controlling the crystal structure and phase transformation by Ba:Ti atomic ratio

Mohammad Reza Mohammadi · A. Esmaeili Rad · D. J. Fray

Received: 16 March 2009 / Accepted: 17 July 2009 / Published online: 29 July 2009

Abstract Highly stable, water-based barium titanate ($BaTiO_3$) sols were developed by a low cost and straightforward sol–gel process. Nanocrystalline barium titanate thin films and powders with various Ba:Ti atomic ratios were produced from the aqueous sols. The prepared sols had a narrow particle size distribution in the range 21–23 nm and they were stable over 5 months. X-ray diffraction pattern revealed that powders contained mixture of hexagonal- or perovskite-$BaTiO_3$ as well as a trace of $Ba_2Ti_{13}O_{22}$ and $Ba_4Ti_2O_{27}$ phases, depending on annealing temperature and Ba:Ti atomic ratio. Highly pure barium titanate with cubic perovskite structure achieved with Ba:Ti = 50:50 atomic ratio at the high temperature of 800 °C, whereas pure barium titanate with hexagonal structure obtained for the same atomic ratio at the low temperature of 500 °C. Transmission electron microscope revealed that the crystallite size of both hexagonal- and perovskite-$BaTiO_3$ phases reduced with increasing the Ba:Ti atomic ratio, being in the range 2–3 nm. Scanning electron microscope analysis revealed that the average grain size of barium titanate thin films decreased with an increase in the Ba:Ti atomic ratio, being in the range 28–35 nm. Moreover, based on atomic force microscope images, $BaTiO_3$ thin films had a columnar-like morphology with high roughness. One of the highest specific surface area reported in the literature was obtained for annealed powders at 550 °C in the range 257–353 m^2g^{-1}.

M. R. Mohammadi · A. E. Rad
Department of Materials Science and Engineering, Sharif University of Technology, Azadi Street, Tehran, Iran

M. R. Mohammadi (✉) · D. J. Fray
Department of Materials Science and Metallurgy, University of Cambridge, Pembroke Street, Cambridge CB2 3QZ, UK
e-mail: mrm41@cam.ac.uk; mohammadi@sharif.edu

Introduction

Materials with submicron and nanosized structures have gained much attention in recent years due to their excellent mechanical, electrical, optical, and magnetic properties. Ceramic and metallic materials characterized by ultrafine crystallite size often display greatly improved performance in comparison to traditional coarse-grained materials. Barium titanate ($BaTiO_3$) is an extensively studied and widely used electroceramic material in various applications. Depending on the transition temperature, $BaTiO_3$ has four kinds of crystal systems, i.e., rhombohedral, orthorhombic, tetragonal, and cubic [1]. The tetragonal phase of $BaTiO_3$ is used in a broad array of electronic devices such as underwater transducers, sensors, and heaters due to its ferroelectric properties, whereas the cubic form, although not ferroelectric, has a high dielectric constant that makes it suitable as capacitors such as multilayer ceramic capacitor (MLCC) [2]. Among them, the high temperature form is the cubic phase with perovskite structure. However, as the temperature is lowered, it goes through successive phase transitions to three different ferroelectric phases, each involving small distortions from the cubic symmetry. At 393 K, it transformed to a tetragonal structure, it is orthorhombic between 278 and 183 K and finally it is rhombohedral below 183 K. Each of these distortions can be thought of as elongations of the cubic unit cell along an edge ([001] or tetragonal), along a face diagonal ([011] or orthorhombic), and along a body diagonal ([111] or rhombohedral) [3]. On the other hand, it has been reported that the phase transition of $BaTiO_3$ from cubic to tetragonal phase is a function of crystallite size as well [1, 4, 5]. The crystal structure becomes less tetragonal as the crystallite size decreases. Thus, there is a critical crystallite size to transform from tetragonal to cubic phase at room

temperature. This critical size depends on the synthetic route and varies in the range 25–200 nm [6].

The traditional preparation method of $BaTiO_3$, reacting between solid phases of BaO or $BaCO_3$ and TiO_2 at temperatures on the order of 1000–1200 °C. However, owing to some limitations of solid-state synthetic, especially in terms of large $BaTiO_3$ grain size with uncontrolled and irregular morphologies and its contamination during repeated calcinations process, several alternative chemical methods have been developed for the synthesis of fine powders [7–9]. Among the various chemical synthesis methods including combustion synthesis, hydrothermal synthesis, chemical coprecipitation, sol–gel route is one of the most widely studied technique [10–13]. However, most of the previous studies focus on non-aqueous systems due to the rapid hydrolysis of a titanium precursor in water. Zhang et al. [14] prepared perovskite-$BaTiO_3$ nanorods by a combined route based on sol–gel and surfactant templated methods using barium acetate and tetrabutyl titanate as the starting materials and laurylamine as the surfactant. Sol–gel $BaTiO_3$ films were produced by Harizanov et al. [15] using tetra ethoxy titanium and barium acetate and acetylacetone as precursors and chelate agent, respectively. Navak et al. [16] used Ti-isopropoxide and Ba-ethoxide for synthesizing $BaTiO_3$ powders. Matsuda et al. [17] and Kumazawa et al. [18] used the similar procedure starting from high-concentration Ba- and Ti-alkoxide precursor solutions and Ba- and Ti-isopropoxide, respectively. Cheung et al. [19] produced $BaTiO_3$ powders by sol–gel process with Ti-isopropoxide and barium acetate precursors. A diol-based sol–gel route for preparing $BaTiO_3$ precursor sols was developed by Tangwiwat [20] using 1,3-propanediol, barium acetate, Ti-isopropoxide, and acetylacetonate. Fujihara et al. [21] investigated interfacial reactions of BaF_2 and TiO_2 in preparing $BaTiO_3$ thin films using a fluoride precursor method. A successful preparation of $BaTiO_3$ by an aqueous sol–gel process should increase the advantages of this method especially for environmental aspects. Lee et al. [22] reported water-based $BaTiO_3$ sol system using barium acetate and titanium bis (ammonium lacto) dihydroxide as precursors and acetic acid as a chelate agent. Although $BaTiO_3$ thin films fired at 550 °C demonstrate a full crystallization, secondary phase of $BaCO_3$ was also observed.

Besides controlling the phase structure, composition homogeneity, crystallite size and monodispersity, and microstructure, the cost of product is an important concern in developing technologies for synthesis of $BaTiO_3$. Therefore, starting with a lower cost precursor such as barium nitrate rather than barium acetate can reduce the total cost for production of $BaTiO_3$. But the main disadvantage of using barium nitrate as a barium precursor is its low solubility in water (e.g., 8.7 g/100 cc at 25 °C [23]) for the aqueous sol–gel process. Guo et al. [24] investigated a Pechini-type precursor system, utilizing Ba-nitrate and Ti-isopropoxide with citric acid and ethylene glycol for synthesis of barium titanate powders. They observed that the prepared precursor solution had limited stability, and some precipitation occurred in the precursor reservoir during the course of powder synthesis. In the present study, a low cost aqueous sol–gel process to synthesis $BaTiO_3$ sol using barium nitrate as a barium source is reported. This aqueous sol–gel process is highly stable and also has potential to produce pure $BaTiO_3$ powders and thin films with nanocrystalline structure without undesirable compounds. Since the performance of $BaTiO_3$ ceramic significantly depends on its phase structure and microstructure, the effect of Ba:Ti atomic ratio on physical characteristics of prepared samples is also studied. So far, no significant study has been reported in this area in the literature.

Experimental

Preparation of the $BaTiO_3$ sols

Titanium tetraisopropoxide (TTIP) with a normal purity of 97% (Aldrich, UK), and barium nitrate ($Ba(NO_3)_2$) with a normal purity of 99% (Aldrich, UK) were used as titanium and barium precursors, respectively. Analytical grade hydrochloric acid (HCl) 37% (Fisher, UK) was used as a catalyst for the peptization and deionized water was used as a dispersing media. Hydroxypropyl cellulose (HPC) with an average molecular weight of 100,000 g mol^{-1} (Acros, USA) was used as a steric stabilizer agent to hinder the crystal growth during annealing heat treatment and preserve microstructure of the films in nanoscale.

A water-based sol–gel process was developed for $BaTiO_3$ systems. The first step was the formation of titanium dioxide sol based on our previous studies [25]. In different beakers, different amounts of $Ba(NO_3)_2$ and HPC were dissolved in deionized water at room temperature and stirred for 30 min to obtain the desirable Ba:Ti atomic ratios, as shown in Table 1. HPC concentration was defined according to previous study [26], which induced the highest surface area. This solution was then mixed with TiO_2 sol, stirring during 2 h.

Table 1 Water-based sol–gel process for $BaTiO_3$ systems with various Ba:Ti atomic ratios

Sample reference	Ba:Ti (at%:at%)	HPC (g/100 mL)
BT31	75:25	1.5
BT11	50:50	1.5
BT13	25:75	1.5

All sols were stable and no gelation occurred during preparation. Sols were characterized in particle size by dynamic light scattering technique (DLS) using a Malvern ZetaSizer 3000HS at 20 °C using a 10 mW He–Ne laser, 633 nm wavelength, and 90° fixed scattering angle. The stability of prepared precursors was also determined with Zeta potential using the same instrument.

Preparation of $BaTiO_3$ thin films

Films were deposited onto 10 × 5×1 mm quartz substrates, in order to avoid TiO_2 peak overlapping with the most commonly used Si and Al substrates in the resulting diffraction pattern. Before deposition, substrates were cleaned using a high power sonic probe consecutively in water, ethanol, and acetone, and dried at 70 °C for 15 min. One layer of film was deposited by dip-coating. The substrates were immersed in the precursor and kept there for a few minutes, followed by a withdrawing speed of 0.6 cm min^{-1}. The subsequent heat treatment was optimized as follows. The films were dried at 150 °C for 1 h, annealed at a rate of 5 °C min^{-1} up to different temperatures (550 and 800 °C) and held at these temperatures for 1 h in air. Drying temperature was defined based on the HPC's glass transition temperature, T_g, which is in the range of 100–150 °C [27]. Drying at T_g is expected to facilitate the decomposition of HPC in the subsequent annealing of the films, since the HPC is transformed to an amorphous state. Films were characterized in microstructure using a scanning electron microscope FE-SEM JEOL 6340 and in topography using atomic force microscope AFM Nanoscope III, Digital Instrument Inc. The average grain size of the films was determined based on scanning electron microscope (SEM) and atomic force microscope (AFM) micrographs.

Synthesis of $BaTiO_3$ powders

Powders were prepared by drying each sol at room temperature for 72 h. Powders were thermally processed in the same way as the films. These powders were characterized in phase composition and crystallite size using an X-ray diffraction diffractometer (XRD) Philips E'pert PW3020, CuK_α and transmission electron microscope (TEM) JEOL 200CX. The crystallite size was calculated by the Debye–Scherrer equation [28]:

$$d = k\lambda/B\cos\theta \quad (1)$$

where d is the crystallite size, k is a constant of 0.9, λ is the X-ray wavelength of Cu which is 1.5406 A°, θ is the Bragg angle in degrees, and B is the full width at half maximum (FWHM) of the peak. Powders were also characterized in thermal behavior using differential scanning calorimetry (DSC) analysis TA-DSCQ2000, with a heating rate of 5 °C min^{-1} in air up to 750 °C; and specific surface area by nitrogen absorption, from Brunauer–Emmett–Teller equation (BET) at 77.3 K using a Micromeritics Tristar 3000 analyzer. Prior to BET measurement, powders were degassed for 24 h at 40 °C with pressure of 0.1 Pa. To prevent any possible crystallization during outgassing, higher drying temperature was avoided. The calculated particle size of the powders from XRD analysis was also verified by BET analysis, using the following equation [29]:

$$d = 6000/s\rho \quad (2)$$

where d (nm) is the average grain size, s (m^2g^{-1}) is the specific surface area, and ρ (gcm^{-3}) is the density of $BaTiO_3$ (6.08 gcm^{-3}).

Results and discussion

Particle size

Figure 1 shows the mean size of the particles for $BaTiO_3$ sols. It can be observed that all sols had a narrow particle size distribution, being 20.5, 21.8, and 22.4 nm for BT31, BT11, and BT13 sols, respectively. Therefore, all sols had nanosized particle resulting from steric stabilization mechanism. The hydrodynamic diameter of the particles in prepared sols is not affected by ionic strength of medium (i.e., the surface charge around the particles) since the equal HCl concentrations were used. The zeta potential of the particles in prepared sols was in the range 40–45 mV (not presented here), which confirmed their good stability against aging. The stability of these sols was achieved by both electrostatic stabilization and steric mechanisms. The electrostatic stabilization mechanism within the sol has effect on particles interaction due to the distribution of

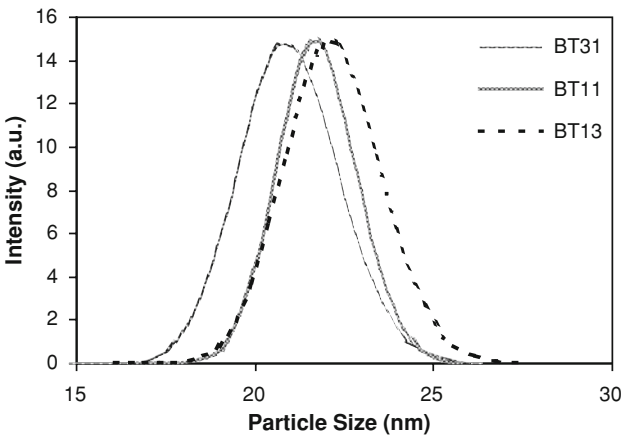

Fig. 1 The mean size of particles in $BaTiO_3$ sols

charged species. The steric repulsion mechanism involves HPC added to the system adsorbing onto the particle surface and preventing the particle surfaces from coming into close contact.

Infrared characteristics

The bond configuration of as-synthesized $BaTiO_3$ powders is shown in Fig. 2. It is known that the absorption bands in the range 1100–1000 cm^{-1} are attributed to the OR groups linked to Ti such as OC_3H_7, OC_4H_7, and OC_2H_5 [30]. The characteristic absorption peak of (OR) group of titanium isopropoxide, which was the precursor of the sols, is in range 1085–1050 cm^{-1} [31]. Owing to the fact that no absorption peak was detected in this range, it is concluded that all four (OR) groups of titanium isopropoxide were substituted with (OH) groups of water. Thus, a full conversion of TTIP is obtained by the hydrolysis reaction, resulting in formation of TiO_2 particles. The weak band at 1383 cm^{-1} is due to the stretching vibration of $\delta(CH_2–CH_3)$ due to the employment of HPC as a PFA. The water incorporation is found with the peak at 1627 cm^{-1}. It is known that the broad band in the range 3220–3097 cm^{-1} is due to the stretching vibration of the hydroxyl (O–H) bond [31].

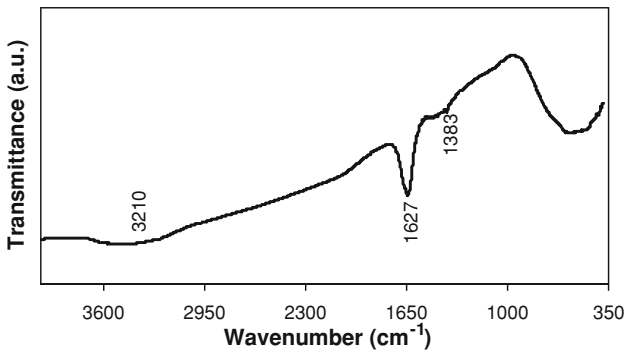

Fig. 2 FTIR spectra of as-synthesized BT31 powder

Crystal characterization

XRD analysis

Figure 3 shows the X-ray diffraction patterns of the powders annealed at 550 and 800 °C for 1 h. Moreover, the distribution of phases determined by XRD is summarized in Table 2. All powders demonstrate a full crystallization after annealing at 550 °C. This is one of the lowest crystallization temperature reported for $BaTiO_3$ in the literature. Highly pure $BaTiO_3$ powder with no undesirable impurities was obtained for the powder containing Ba:Ti atomic ratio of 50:50 (i.e., BT11). The titanium prominent powder (i.e., Ba:Ti < 50:50) showed a mixture of $BaTiO_3$ and $Ba_2Ti_{13}O_{22}$ [matched with JCPDS database number of 81-2092] phases. This powder (BT13) showed more than 92 and 82% $BaTiO_3$ phase at annealing temperatures of 550 and 800 °C, respectively. The barium prominent powder (i.e., Ba:Ti > 50:50) was a mixture of $BaTiO_3$ and

Table 2 Phase distribution of prepared powders determined by X-ray diffraction

Powder	550 °C	800 °C
BT31	$BaTiO_3$ (H) + $Ba_4Ti_2O_{27}$	$BaTiO_3$ (CP) + $Ba_4Ti_2O_{27}$
BT11	$BaTiO_3$ (H) + $BaTiO_3$ (CP)	$BaTiO_3$ (H) + $BaTiO_3$ (CP)
BT13	$BaTiO_3$ (H) + $Ba_2Ti_{13}O_{22}$	$BaTiO_3$ (CP) + $Ba_2Ti_{13}O_{22}$

H Hexagonal-$BaTiO_3$, *CP* Cubic perovskite-$BaTiO_3$

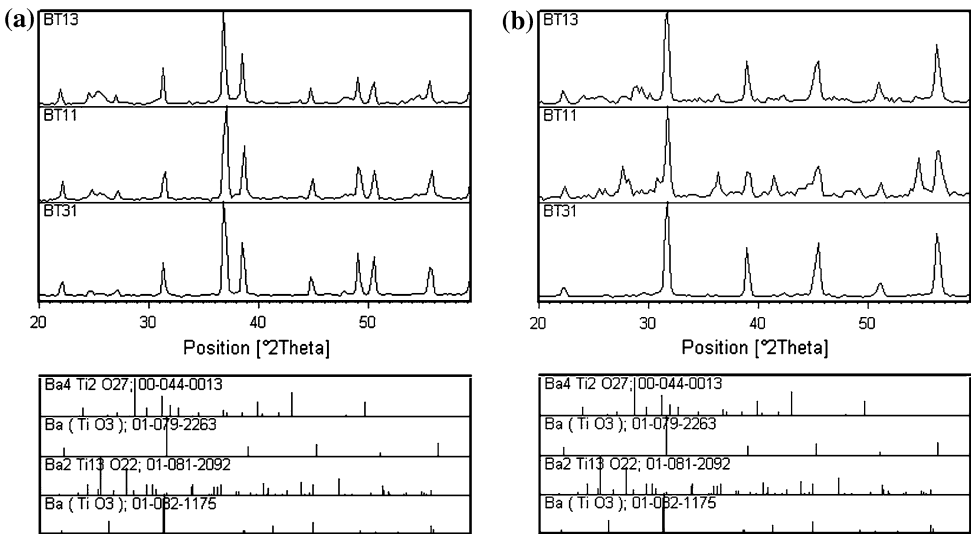

Fig. 3 XRD pattern of BT31, BT11, and BT13 powders annealed at: **a** 550 °C and **b** 800 °C for 1 h

$Ba_4Ti_2O_{27}$ [matched with JCPDS database number of 44-0013]. Barium titanate content of this powder (BT31) was around 98%. It is worth to note that, $BaTiO_3$ with hexagonal structure and lattice parameter of $a = 5.73$ A° and $c = 14.05$ A° [matched with JCPDS database number of 82-1175] formed at 550 °C, while after annealing at 800 °C it transformed to cubic perovskite-$BaTiO_3$ with lattice parameter of $a = b = c = 3.99$ A° [matched with JCPDS database number of 79-2263]. Therefore, hexagonal-$BaTiO_3$ to perovskite-$BaTiO_3$ phase transformation was occurred with increasing annealing temperature. Cho [32] reported hexagonal-$BaTiO_3$ phase in the powders prepared from organic precursor. He described formation of hexagonal phase based on the stacking sequence in the regions of the defects that was similar to that of the high-temperature hexagonal-$BaTiO_3$. The planar defects can be formed due to the complex phenomena associated with Ti^{+3} and oxygen and/or barium vacancies. The similar explanation can be expressed in our case due to the presence of anatase phase, which has some Ti^{3+} states (oxygen defects) [33], for 500 °C annealed powders.

It has been reported that tetragonal-$BaTiO_3$ has two separate peaks between 2θ 44° and 47°, and complete cubic-$BaTiO_3$ shows just one peak [12]. Since one peak was observed in this range, the crystal structure of 800 °C annealed powder was determined cubic-$BaTiO_3$. The hexagonal-$BaTiO_3$ phase was exhibited by the strongest peaks at $2\theta = 36.9°$ (201) and $2\theta = 38.5°$ (202), whilst cubic perovskite-$BaTiO_3$ phase was revealed by the strongest peaks at $2\theta = 317°$ (101) and $2\theta = 56.2°$ (112). The preferential orientation of hexagonal-$BaTiO_3$ phase was along (201) direction but it was along (111) direction for perovskite-$BaTiO_3$ phase.

Consequently, in the present article pure $BaTiO_3$ with cubic perovskite structure was produced successfully by a simple and low cost water-based sol–gel process aided by barium nitrate as a barium source.

Effect of Ba:Ti atomic ratio on crystallite size of the powders annealed at 550 and 800 °C is shown in Fig. 4. It is evident that the average crystallite size of powders is in the range 2–3 nm at all annealing temperatures. In addition, powders showed good thermal stability against annealing heat treatment, since a gradual increase was occurred after annealing at 800 °C. As mentioned earlier, tetragonal to cubic phase transformation occurs with decreasing the crystallite size of $BaTiO_3$. Since the 800 °C annealed powders had an ultrafine crystallite size, they showed cubic perovskite structure.

Zhang et al. [14] prepared $BaTiO_3$ nanorods with cubic perovskite structure and 30 nm crystallite size at 450 °C by a combined route based on sol–gel and surfactant templated methods. Barium titanate powder with crystallite size of 50 nm annealed at 1100 °C was prepared by Navak et al.

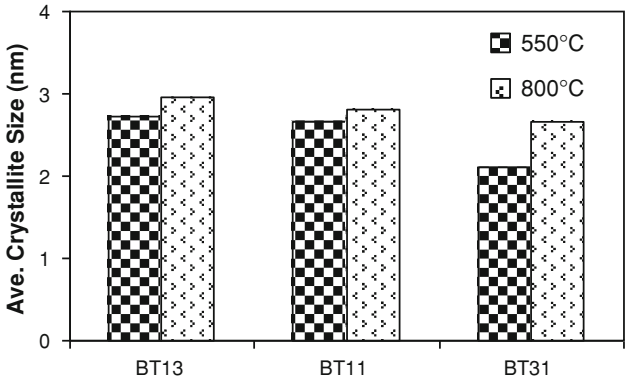

Fig. 4 Effect of Ba:Ti atomic ratio on crystallite size of annealed powders

[16]. Barium titanate thin film produced by Harizanov et al. [15] showed full crystallization at 800 °C with cubic structure and it transformed to tetragonal phase at 1000 °C. Lee et al. [22] synthesized crystalline $BaTiO_3$ powder at 550 °C containing $BaCO_3$ secondary phase. The pure powder was obtained at 800 °C with cubic perovskite structure. Kumazawa et al. [18] observed that full crystallization of sol–gel $BaTiO_3$ film, with crystallite size of 25 nm, occurred in the range 800–900 °C, containing $Ba_5Ti_{17}O_4$ phase. Cheung et al. [19] prepared sol–gel crystalline $BaTiO_3$ powder with tetragonal structure and crystallite size of 30 nm at 800 °C. Sol–gel $BaTiO_3$ powder with cubic perovskite system and 31 nm crystallite size was obtained at 700 °C by Wang et al. [10]. They observed that the average crystallite size of the powder increased up to 43 nm using barium stearate rather than barium acetate. Tangwiwat et al. [20] synthesized sol–gel $BaTiO_3$ powder with secondary phases of $BaCO_3$ and Ba_2TiO_4 at annealing temperature of 600 and 900 °C, respectively. They obtained pure $BaTiO_3$ powder at 1000 °C. Kim et al. [1] produced cubic $BaTiO_3$ powder with average particle size of 100 nm by hydrothermal method. Guo et al. [24] synthesized crystalline $BaTiO_3$ powder containing $Ba_2Ti_2O_5CO_3$, $BaCO_3$, and $Ba(NO_3)_2$ secondary phases at 700 °C. The pure powder was produced by increasing annealing temperature up to 800 °C. Therefore, in the present study not only highly pure perovskite $BaTiO_3$ powder was synthesized with a water-based sol–gel process, but also one of the smallest crystallite size reported in the literature was obtained. Furthermore, the crystallization temperature of synthesized powder is lower than that of reported in previous studies.

TEM analysis

Figure 5 highlights the selected area diffraction pattern (SADP) of BT11 powder annealed at 550 °C for 1 h. As seen, prepared powder exhibited high uniformity in particle size and shape. Moreover, the obtained typical well-defined

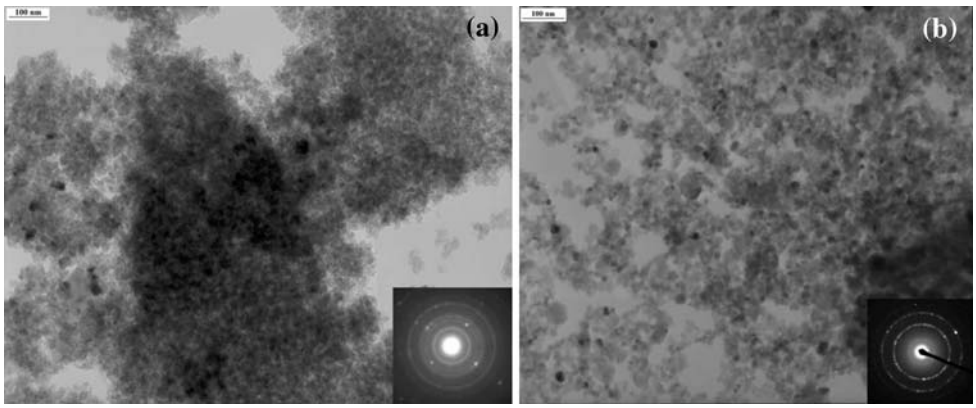

Fig. 5 TEM analysis of BT11 powder: **a** bright-field plane-view image after annealing at 550 °C and **b** bright-field plane-view image after annealing at 800 °C, inset shows the typical well-defined rings arising from crystallite structure

rings, as shown inset, arise from crystallite structures. The relative electron diffraction pattern indicates a random orientation for the polycrystalline powder. The average crystallite size of the powders is around 2–3 nm, which is consistent with those obtained by XRD analysis.

Thermal analysis

Differential scanning calorimetry (DSC) analysis of BT31 powder is shown in Fig. 6. The addition of HPC into sol influences the process of organic decomposition that is shown by the first sharp exothermic peak in the range 240–336 °C (with maximum at 300 °C). This exothermic reaction was reported previously for sol–gel derived TiO_2-based powders [34]. The second small and broad exothermic peak in the range 392–420 °C (with maximum at 400 °C) shows the initial crystallization of hexagonal-$BaTiO_3$. Barium nitrate is known to decompose close to its melting point, which is around 552 °C. Therefore, the third endothermic peak in the range 548–568 °C (with maximum at 556 °C) shows decomposing of barium nitrate. Decomposition of barium nitrate continues in the next step that is revealed by an endothermic in the range 600–656 °C (with maximum at 638 °C). Finally the last exothermic peak appeared in the range 656–712 °C (with maximum at 704 °C) is attributed to hexagonal to cubic perovskite phase transformation of $BaTiO_3$.

Figure 7 shows the results of thermogravimetric analysis (TGA) of BT31 powder. As seen, the weight loss occurs at four stages. In the first stage (up to 340 °C), the weight loss

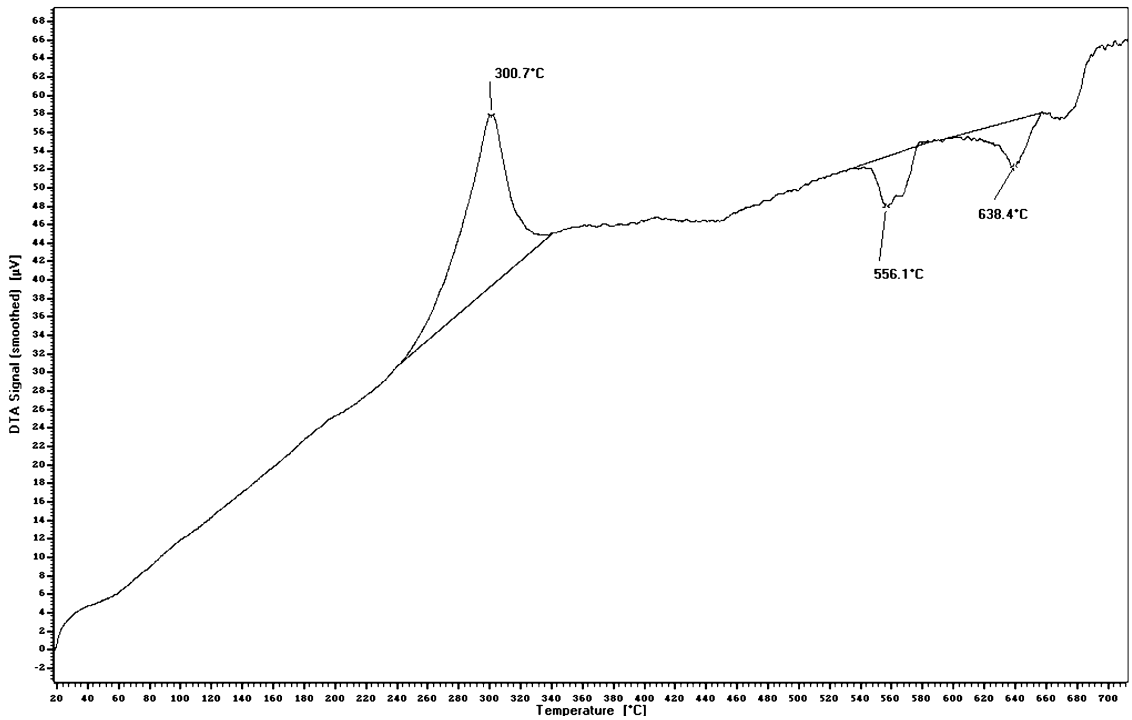

Fig. 6 DSC curve of BT31 powder dried at room temperature for 72 h. The scan rate was 5 °C min^{-1}, performed in air

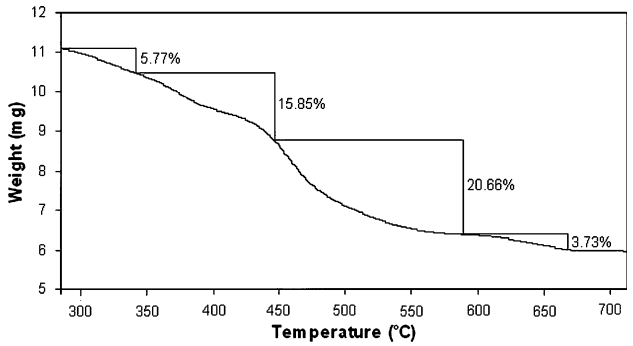

Fig. 7 TGA curve of BT31 powder dried at room temperature for 72 h. The scan rate was 5 °C min^{-1}, performed in air

is ascribed to the decomposition of HPC and inorganic component. Decomposition of residual HPC and inorganic component occur in the second stage, from 340 to 450 °C. In the third and fourth stages, in the temperature ranges 450–590 °C and 590–670 °C, respectively, the weight losses are attributed to decomposition of barium nitrate. No weight loss occurs at temperatures higher than 670 °C, is considered as hexagonal to cubic perovskite phase transformation of $BaTiO_3$.

Microstructure

FE-SEM analysis

Figure 8 shows micrographs of BT31, BT11, and BT13 thin films annealed at 550 °C. In all cases relatively dense, crack-free, homogeneous, and nanograined films were obtained. The interstices between the particles are noticeable, resulting in mesoporous structure. The porosity of the films reduced with increasing Ba:Ti atomic ratio. This can be explained by the fact that barium nitrate decomposition

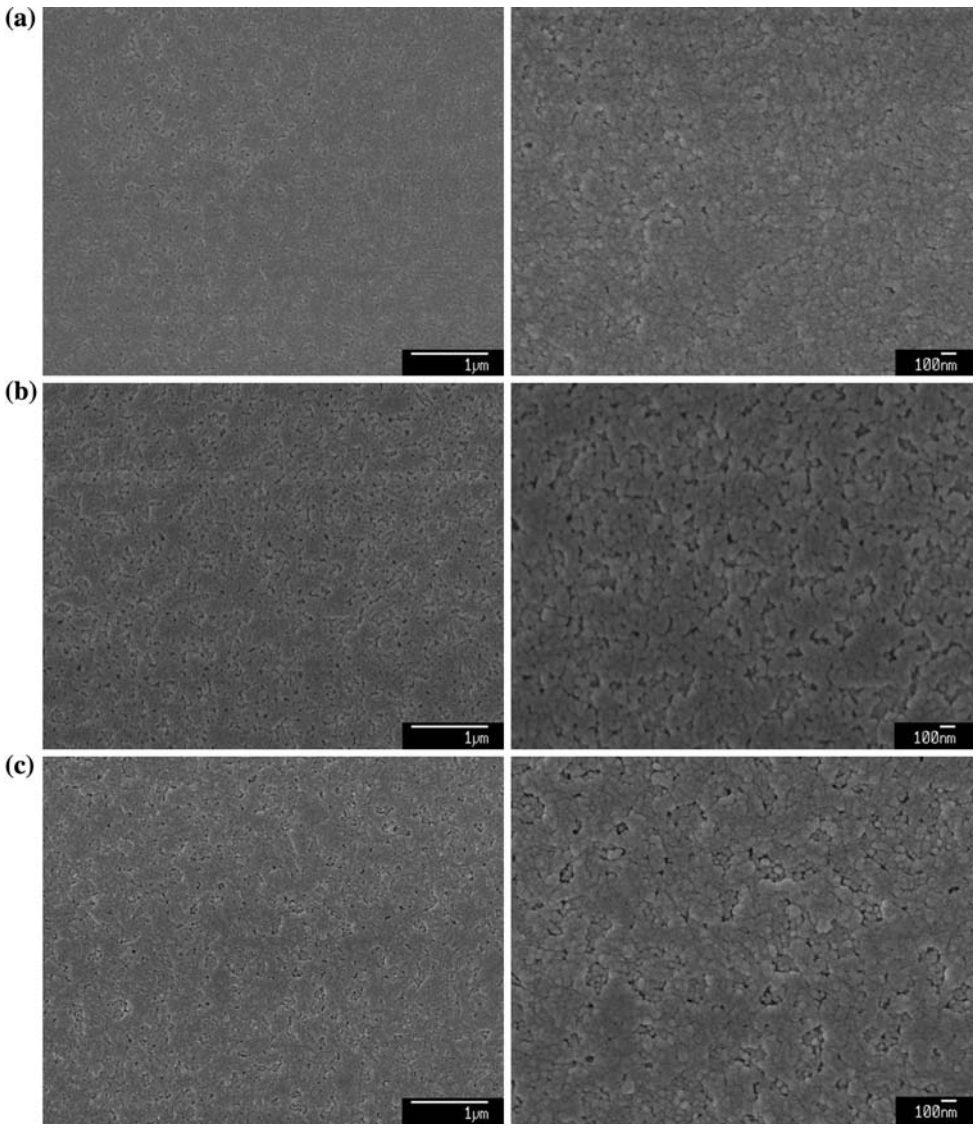

Fig. 8 $BaTiO_3$ morphology of the films annealed at 550 °C as a function of component composition change: **a** BT31, **b** BT11, and **c** BT13

is an exothermic process and heat released help sintering the particles. Based on the SEM images in high magnification (not shown here), it was concluded that the average grain size of $BaTiO_3$ films was 28 nm for BT31, 33 nm for BT11, and 35 nm for BT13. Thus, BT31 film annealed at 550 °C had the smallest grain size among all films. This result is consistent with the average crystallite size of the samples obtained by XRD analysis.

In addition, it is concluded that HPC plays an essential role during grain growth. It is adsorbed onto the $BaTiO_3$ particles and act as in situ steric stabilizer, preventing particle sintering and film from cracking during the annealing treatment.

The cross-sectional SEM micrograph (not shown here) revealed that thickness of $BaTiO_3$ films was in the range 150–200 nm, respectively. The thickness of the thin films decreased with increasing Ba:Ti atomic ratio. The same parameters, such as withdrawing speed and angle, were selected during film preparation. Thus, the only parameter can effect on thickness of the films is the viscosity of the sols. Indeed barium prominent sol (i.e., BT31) had the lowest viscosity among all sols.

Fujihara et al. [21] studied the effect of additives such as acetylacetone and trifluoroacetic acid on morphology of sol–gel $BaTiO_3$ films. They found that acetylacetone decreased the grain size of the films, whereas trifluoroacetic acid reduced the grain boundaries. Barium titanate films consisted of the nanoscale polycrystallites with grain size of 30–60 nm at 800 °C reported by Lee et al. [22]. Matsuda et al. [17] prepared smooth $BaTiO_3$ films with no

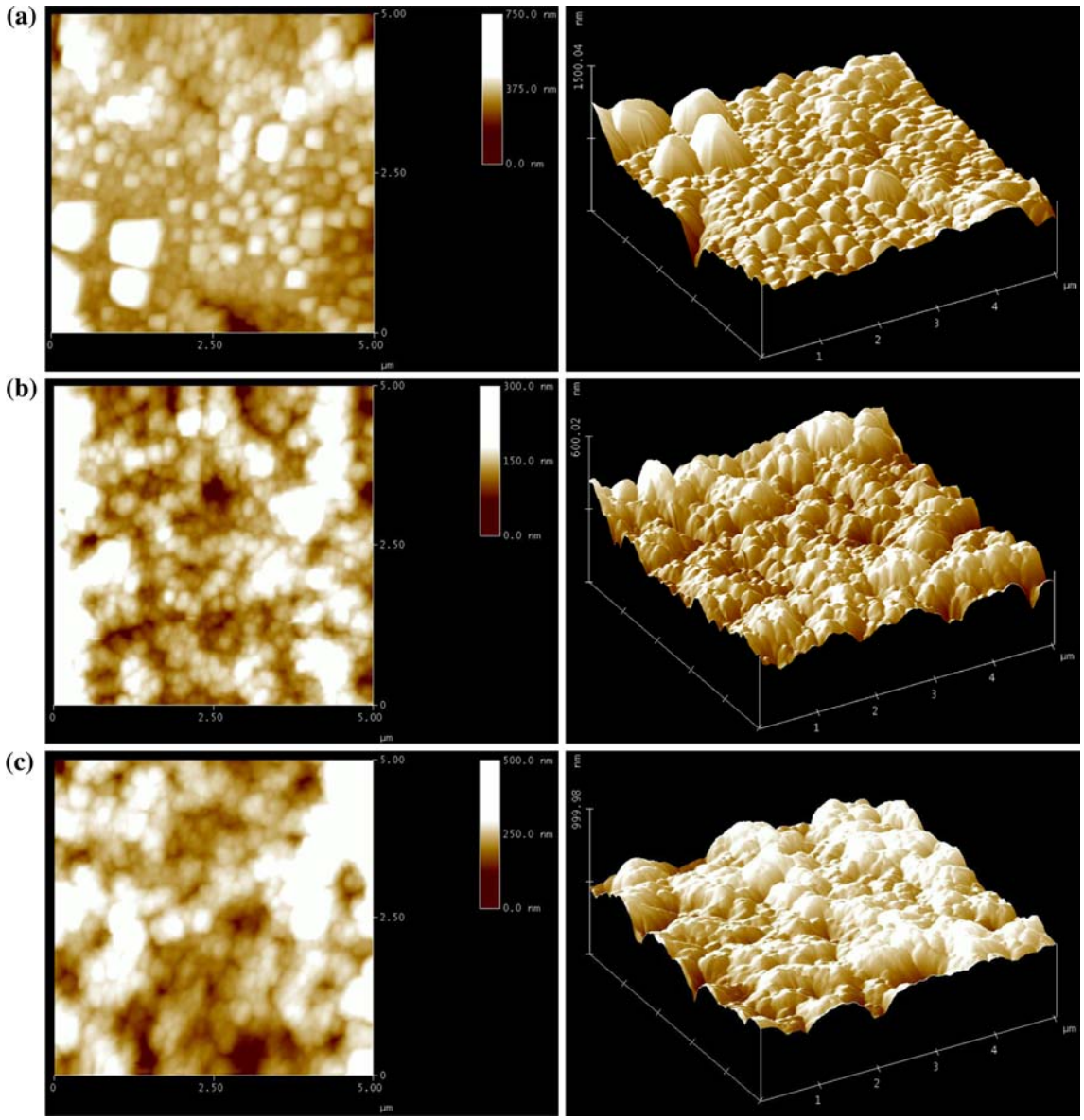

Fig. 9 Atomic force micrographs of 550 °C annealed films: **a** BT31, **b** BT11, and **c** BT13

pores or cracks by sol–gel and spin coating methods. Therefore, we succeeded to produce $BaTiO_3$ thin films with one of the smallest grain size reported in the literature so far. In addition, the microstructure of $BaTiO_3$ films was found to be significantly dependant upon preparation method and Ba:Ti atomic ratio.

AFM analysis

Figure 9 shows 2D and 3D topographies of $BaTiO_3$ thin films annealed at 550 °C for 1 h.

All samples show that the films are homogeneous, rough, and uniform with nanosized grains. Moreover, they had a columnar-like morphology. The average grain size of the films was 30, 34, and 37 nm for BT31, BT11, and BT13, respectively. These results are in good agreement with those obtained by SEM images. The roughness mean square (rms) of the films, obtained on 5 μm × 5 μm scan area, was 37, 62, and 48 nm.

Dicken et al. [35] investigated the growth of $BaTiO_3$ thin films on MgO substrate by molecular beam epitaxy (MBE). AFM analysis revealed that the grain size of the film was on the order of 200 nm and rms roughness was 2 nm for a 60 μm × 60 μm scan area. Canulescu et al. [36] grown $BaTiO_3$ film on Pt-coated Si substrates by radio-frequency discharge assisted pulsed laser deposition (RF-PLD). They found that a significant reduction of surface roughness was occurred at higher RF power (200 W in respect to 100 W). The roughness of 147 nm was obtained for 200 W RF power on 40 μm × 40 μm scan area.

Specific surface area

Figure 10 illustrates the N_2 adsorption–desorption isotherms of annealed powders at 550 °C. The isotherm of the powders represents a combination of types III and V corresponds to either mesoporous materials (pore diameter >2 nm) or macroporous materials (pore diameter >50 nm) [37]. The effect of Ba:Ti molar ratio on specific surface

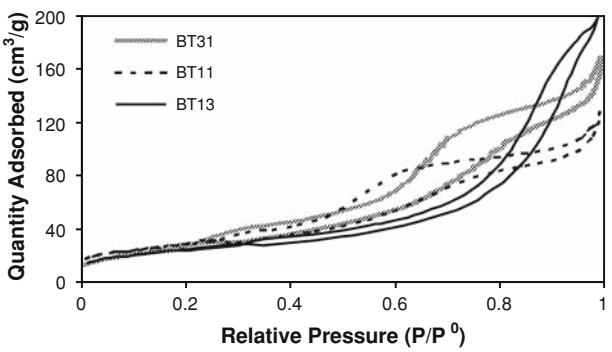

Fig. 10 Nitrogen adsorption–desorption isotherm of annealed powders at 550 °C

Table 3 N_2 adsorption–desorption characteristics of annealed powders at 550°C

Sample	S_{BET} (m^2g^{-1})	V_{Tot} (cm^3g^{-1})	P_{BET} (nm)	d (nm)
BT31	353	0.12	2.2	2.8
BT11	286	0.10	2.5	3.4
BT13	257	0.10	2.5	3.8

S_{BET} BET specific surface area, V_{Tot} total pore volume calculated by BET method at $P/P^0 = 0.99$, P_{BET} pore size calculated by BET method, d particle size calculated by Eq. 2

area, pore volume, and pore size of the powders is summarized in Table 3. It can be observed that all powders have a mesoporous structure due to the pore diameter greater than 2 nm. As expected, BT31 powder had the highest surface area among the powders annealed at 550 °C. This result was also confirmed by those obtained by XRD analysis, since this powder showed the smallest crystallite size among the powders annealed at 550 °C. As seen, the particle size of the powders is in the range 2.8–3.8 nm which is in good agreement with those obtained by XRD and TEM analyses.

Conclusions

Nanostructured and mesoporous pervoskite-$BaTiO_3$ thin films and powders have been successfully prepared via a water-based sol–gel route. Titanium isopropoxide and barium nitrate were used as titanium and barium precursors, and HPC used as a steric stabilizer agent. Prepared sols with various Ba:Ti atomic ratios had particle size in the range 23–26 nm and stability over 5 months, confirmed by zeta potential analysis. Depending on Ba:Ti atomic ratio the mixtures of $BaTiO_3$ and $Ba_2Ti_{13}O_{22}$ and $BaTiO_3$ and $Ba_4Ti_2O_{27}$ phases were observed for the powders containing Ba:Ti < 50:50 and Ba:Ti > 50:50 atomic ratios, respectively. Highly pure $BaTiO_3$ phase obtained for the powders containing Ba:Ti = 50:50 atomic ratio. XRD and DSC results showed that the hexagonal to perovskite phase transformation occurred with increasing annealing temperature around 700 °C. Barium titanate with the cubic perovskite system obtained for the powders annealed at high temperature of 800 °C, whereas $BaTiO_3$ with hexagonal system achieved for the powders annealed at low temperature of 500 °C. SEM images revealed that relatively dense, crack-free, homogeneous, and nanograins films were obtained. Based on AFM analysis for annealed films at 550 °C, BT31 had the smallest average grain size (37 nm), whereas BT11 showed the highest roughness mean square (62 nm on 5 μm × 5 μm scan area). BET analysis confirmed that the isotherm corresponding to the annealed powders represented a combination of types III

and V corresponds to mesoporous materials. The highest surface area of 353 m^2g^{-1} was measured for BT31-550 °C.

Acknowledgement The authors wish to acknowledge Mr. David Nicol for his help with TEM analysis.

References

1. Kim YI, Jung JK, Ryu KS (2004) Mater Res Bull 39:1045
2. Hu MZC, Payzant VKEA, Rawn CJ, Hunt RD (2000) Powder Technol 110:2
3. Kwei GH, Lawson AC, Billinge SJL (1993) J Phys Chem 97:2368
4. Kwon SW, Yoon DH (2007) J Eur Ceram Soc 27:247
5. Kwon SW, Yoon DH (2007) Ceram Int 33:1357
6. Yen FS, Hasing HL, Chang YH (1995) Jpn J Appl Phys 34:6149
7. Ihlefeld JF, Borland WJ, Maria JP (2008) J Mater Sci 43:4264. doi:10.1007/s10853-008-2618-x
8. Yaseen H, Baltianski S, Tsur Y (2007) J Mater Sci 42:9679. doi:10.1007/s10853-007-1944-8
9. Hung KM, Hsieh CS, Yang WD, Sun YJ (2007) J Mater Sci 42:2376. doi:10.1007/s10853-006-1452-2
10. Wang L, Liu L, Xue D, Kang H, Liu C (2007) J Alloys Compd 440:78
11. Ischenko V, Pippel E, Köferstein R, Abicht HP, Woltersdorf J (2007) Solid State Sci 9:21
12. Baeten F, Derks B, Coppens W, van Kleef E (2006) J Eur Ceram Soc 26:589
13. Jhung SH, Lee JH, Yoon JW, Hwang YK, Hwang JS, Park SE, Chang JS (2004) Mater Lett 58:3161
14. Zhang S, Jiang F, Qu G, Lin C (2008) Mater Lett 62:2225
15. Harizanov O, Harizanova A, Ivanova I (2004) Mater Sci Eng B106:191
16. Novak Z, Knez Z, Ban I, Drofenik M (2001) J Supercrit Fluids 19:209
17. Matsuda H, Kobayashi N, Kobayashi T, Miyazawa K, Kuwabara M (2000) J Non-Cryst Solids 271:162
18. Kumazawa H, Masuda K (1999) Thin Solid Films 353:144
19. Cheung MC, Chan HLW, Zhou QF, Choy CL (1991) Nanostruct Mater 11:837
20. Tangwiwat S, Milne SJ (2005) J Non-Cryst Solids 351:976
21. Fujihara S, Schneller T, Waser R (2004) Appl Surf Sci 221:178
22. Lee B, Zhang J (2001) Thin Solid Films 388:107
23. Lide DR (2007) Handbook of chemistry and physics, 87th edn. CRC Press, Ohio, p 4
24. Guo W, Datye AK, Ward TL (2005) J Mater Chem 15:470
25. Mohammadi MR, Cordero-Cabrera MC, Ghorbani M, Fray DJ (2006) J Sol–Gel Sci Technol 40:15
26. Mohammadi MR, Cordero-Cabrera MC, Fray DJ, Ghorbani M (2006) Sens Actuators B: Chem 120:86
27. Kishi A, Toraya H (2004) Rigaku J 21:25
28. Cullity BD (1978) Elements of X-ray diffraction. Addison-Wesley Publishing Company, Inc., London, p 99
29. Liu X, Yang J, Wang L, Yang X, Lu L, Wang X (2000) Mater Sci Eng A 289:241
30. Ivanova T, Harizanova A, Surtchev M (2002) Mater Lett 55:327
31. Socrates G (1994) Infrared characteristic group frequencies: tables and charts. Wiley, England, p 6 (62 and 237)
32. Cho WS (1998) J Phys Chem Solids 59:659
33. Takaoka GH, Hamamo T, Fukushima K, Matsuo J, Yamada I (1997) Nucl Instr Meth Phys Res B 121:503
34. Mohammadi MR, Fray DJ (2007) Acta Mater 55:4455
35. Dicken MJ, Diest K, Park YB, Atwater HA (2007) J Cryst Growth 300:330
36. Canulescu S, Dinescu G, Epurescu G, Matei DG, Grigoriu C, Craciun F, Verardi P, Dinescu M (2004) Mater Sci Eng B 109:160
37. Webb PA, Orr C (1997) Analytical methods in fine particle technology. Micromeritics Instrument Corporation, USA, p 55